Journal of Nuclear Medicine, published on December 15, 2016 as doi:10.2967/jnumed.116.182824

In-vivo PET imaging of the "cancer integrin" αvβ6 using gallium-68 labelled cyclic RGD nonapeptides

Johannes Notni[1], Dominik Reich[1], Oleg V. Maltsev[2], Tobias G. Kapp[2], Katja Steiger[3], Frauke Hoffmann[1], Irene Esposito[4], Wilko Weichert[3], Horst Kessler[2], Hans-Jürgen Wester[1]

1 *Lehrstuhl für Pharmazeutische Radiochemie, Technische Universität München, Walther-Meissner-Strasse 3, D-85748 Garching, Germany, E-mail: johannes.notni@tum.de, Homepage: http://www.prc.ch.tum.de*

2 *Institute for Advanced Study and Center of Integrated Protein Science (CIPSM), Department Chemie, Technische Universität München, Munich, Germany*

3 *Institute of Pathology, Technische Universität München, Munich, Germany*

4 *Institute of Pathology, Universitätsklinikum Düsseldorf, Düsseldorf, Germany*

Corresponding Author:

Johannes Notni

Lehrstuhl für Pharmazeutische Radiochemie

Technische Universität München

Walther-Meissner-Strasse 3

D-85748 Garching

Germany

email address: johannes.notni@tum.de

tel: +498928910266 / fax: +498928912204

Running title: PET imaging of αvβ6 integrin

Word count: 5051

ABSTRACT

Expression of the cellular transmembrane receptor αvβ6 integrin is essentially restricted to malignant epithelial cells in carcinomas of a broad variety of lineages, while it is virtually absent in normal adult tissues. Thus, it is a highly attractive target for tumor imaging and therapy. Furthermore, αvβ6 integrin plays an important role for the epithelial-mesenchymal interaction and the development of fibrosis. **Methods:** On the basis of the Gallium-68 chelators TRAP (triazacyclononane-triphosphinate) and NODAGA, we synthesized mono- di- and trimeric conjugates of the αvβ6 integrin-selective peptide cyclo(FRGDLAFp(*N*Me)K) via click chemistry. These were labeled with gallium-68 and screened regarding their suitability for in-vivo imaging of αvβ6 integrin expression by positron emission tomography (PET) and ex-vivo biodistribution in SCID mice bearing H2009 tumor (human lung adenocarcinoma) xenografts. For these, αvβ6 integrin expression in tumor and other tissues was determined by β6 immunohistochemistry. **Results:** Despite the multimers showed higher αvβ6 integrin affinities (23–120 pM) than the monomers (260 pM), best results, that is, low background uptake and excellent tumor delineation, were obtained with the TRAP-based monomer ^{68}Ga-Avebehexin. This compound showed the most favourable pharmacokinetics due to its high polarity (log D = –3.7) and presence of additional negative charges (carboxylates) on the chelator, promoting renal clearance. Although tumor uptake was low (0.65 ± 0.04 % injected dose per gram tissue, %ID/g), it was still higher than in all other organs except the kidneys, ranging from a maximum for the stomach (0.52 ± 0.04 % ID/g) to almost negligible for the pancreas (0.07 ± 0.01% ID/g). A low but significant target

expression in tumor, lung and stomach was confirmed by immunohistochemistry. **Conclusion:** Because of highly sensitive PET imaging even of tissues with low αvβ6 integrin expression density, we anticipate clinical applicability of ^{68}Ga-Avebehexin for imaging of αvβ6 tumors and fibrosis by PET.

Keywords: Positron emission tomography, Gallium-68, Click Chemistry, preclinical imaging

INTRODUCTION

The cellular transmembrane receptor αvβ6 integrin is one of eight integrins recognizing the arginine-glycine-aspartate (RGD) peptide sequence, a structural motif mediating cellular adhesion to a variety of extracellular matrix proteins, such as vitronectin and fibronectin (*1*). In contrast to other popular RGD-binding integrins, such as αvβ3 and α5β1, which are expressed by different cell types and have gained considerable attention due to their involvement in formation and sprouting of blood- and lymphatic vessels (vascularisation, angiogenesis and lymphangiogenesis) (*2*), αvβ6 integrin levels in adult tissues are generally very low (*3*). Expression of αvβ6 integrin is restricted to epithelial cells (*4*), which is already pointing to a potential relevance for tumor management because the majority of malignant neoplasms (85%) are carcinomas (*5*), that is, tumors of epithelial origin. Indeed, many carcinomas show an enhanced αvβ6 integrin expression (*6*), for example, pancreatic (*7*), cholangiocellular (*8*), gastric (*9*,*10*), breast (*11*) ovarian (*12*,*13*) colon (*14*) and those of the upper aereodigestive tract (*15*). αvβ6 integrin has furthermore been described as a marker for increased invasiveness and malignancy of several carcinomas and thus, poor prognosis (*6,9,12,14*). As such, the "cancer integrin" αvβ6 is a very attractive target for specific tumor imaging and therapy. Beyond that, it plays an important role in the epithelial-mesenchymal interaction, e.g., during development of biliary (*16*), renal (*17*) as well as pulmonary (*18*) fibrosis.

This has prompted research on αvβ6-specific, non-peptidic (*19*) as well as peptidic inhibitors (*20,21,22,23*). Such compounds, e.g., the linear peptides A20FMDV2

(sequence: NAVPNLRGDLQVLAQKVART, derived from foot-and-mouth disease virus, FMDV) (*21*), H2009.1 (seq.: RGDLATLRQL) (*22*) and the cyclic peptide $S_0$2 (*23*) were equipped with radiolabels and applied for in-vivo imaging of αvβ6 expression (*24*) by single-photon emission computed tomography (SPECT) (*25,26,27*) and positron emission tomography (PET) (*21,28,29,30,31,32*). More recently, efforts directed at further downsizing and metabolic stabilization of FMDV-peptide derived αvβ6 integrin ligands led to discovery of the cyclic nonapeptide cyclo(FRGDLAFp(*N*Me)K) (*33*), which exhibits high αvβ6 binding affinity (0.26 nM), remarkable selectivity against other integrins (αvβ3: 632 nM; α5β1: 73 nM; αvβ5 and αIIbβ3: >1 μM), and full stability in human plasma up to 3 h. In addition, its activity was not compromised by functionalization on the lysine side chain, rendering it an optimal starting point for elaboration of molecular probes.

We aimed at the corresponding probes for application in PET imaging, labeled with Gallium-68 ($t_{½}$ = 68 min), which is conveniently available from ^{68}Ge/^{68}Ga generators (small benchtop devices acting as long-lived regenerative sources for $^{68}Ga^{III}$ in dilute HCl). For ^{68}Ga radiolabeling, the peptide must be equipped with a chelator capable of binding the radiometal ion into a kinetically inert complex. For this purpose, we selected the chelator TRAP (*34*) (1,4,7-triazacyclononane-1,4,7-tris[methylene(2-carboxyethyl)]phosphinic acid (*35*), because its extraordinary affinity to (*36,37,38*) and selectivity for (*39,40,41*) gallium radionuclides enables highly efficient and reliable radiolabeling procedures (*42*). Due to presence of three independent sites for conjugation, TRAP allows for facile attachment of additional reporter molecules (*43*) or multimerization of targeting vectors (*44*), which is particularly conveniently done by

means of click chemistry, that is, copper-catalyzed alkyne-azide cycloaddition (CuAAC) (*45*).

MATERIALS & METHODS

Syntheses and analytical characterization of the novel compounds is described in the Supplemental material.

Integrin αvβ6 Affinities

Integrin binding assays were performed as described previously (*33*) by enzyme linked immune sorbent assays. Briefly, 96-well plates were coated with latency-associated peptide (transforming growth factor β) as extracellular matrix protein. Free binding sites were blocked by incubation with bovine serum albumin. Solutions of the respective compounds were added, followed by a solution of the integrin. Surface bound integrin was detected by subsequent incubation with a primary antibody (mouse-anti-human) and a second antibody-peroxidase conjugate (anti-mouse horseradish peroxydase). After addition of the dye tetramethylbenzidine and quenching of the reaction by addition of sulphuric acid, the absorbance signal at $\lambda = 405$ nm was measured. The determined IC_{50} value for the inhibitor is referenced to the internal standard RTD_lin (linear helical RTD-peptide RTDLDSLRT) with an αvβ6-binding affinity of 33 nM.

Radiochemistry

^{68}Ga labeling was done using an automated system (GallElut^{+} by Scintomics, Germany) as described previously (*36*). Briefly, non-processed eluate of a ^{68}Ge/^{68}Ga-

generator with SnO_2 matrix (by IThemba LABS, SA; 1.25 mL, eluent: 1 M HCl, total ^{68}Ga activity 500 MBq) was adjusted to pH 2 by adding 4-(2-hydroxyethyl)-1-piperazineethanesulfonic acid buffer solution (450 µL of a 2.7 M solution, prepared from 14.4 g 4-(2-hydroxyethyl)-1-piperazineethanesulfonic acid and 12 mL water) and used for labeling of 0.5 nmol of the respective chelator conjugate for 3 min at 95 °C. Purification was done by passing the reaction mixture over a C8 light solid phase extraction cartridge (SepPak), which was purged with water (10 mL) and the product eluted with an ethanol/water mixture (1:1 by volumes, 1 mL). Purity of the radiolabeled compounds was determined by radio-TLC (eluents: aq. acetate solution or citrate solution).

Cell Lines and Animal Models

All animal studies have been performed in accordance with general animal welfare regulations in Germany and the institutional guidelines for the care and use of animals. H2009 human lung adenocarcinoma cells (CRL-5911; American Type Culture Collection, Manassas, VA, USA) were cultivated as recommended by the distributor. To establish tumor xenografts, 6 to 8 weeks old female CB17 severe combined immunodeficiency mice (Charles River, Sulzfeld, Germany) were inoculated with 10^7 H2009 cells in Matrigel (CultrexBME, Type 3 PathClear, Trevigen, GENTAUR GmbH, Aachen, Deutschland). Mice were used for biodistribution or PET studies when tumours had grown to a diameter of 6–8 mm (3–4 weeks after inoculation).

Biodistribution and PET Imaging

Animals were injected 12–15 MBq (for PET) or 5–7 MBq (for biodistribution studies) of the radiotracers under isoflurane anaesthesia and subsequently allowed to wake up with access to food and water. For blockade, 60 nmol of the respective unlabeled compound was administered 10 min before tracer injection. For biodistribution, animals were sacrificed after 90 min, organs harvested, weighed and the activity contained therein counted in a gamma-counter (Perkin-Elmer). Calculation of injected dose per gram tissue was done from organ weights and counted activities, based on individually administered doses. PET was recorded under isoflurane anaesthesia 60 or 75 min p.i. for 20 min on a Siemens Inveon small-animal PET system. Images were reconstructed as single frames using Siemens Inveon software, employing a three-dimensional ordered subset expectation maximum algorithm without scatter and attenuation correction.

Immunohistochemistry

For histology and immunohistochemistry, animals were sacrificed immediately after PET imaging. Tumour tissue and representative organs were fixed in 10% neutral-buffered formalin, routinely embedded in paraffin, and cut in 2 µm sections. Hematoxylin-eosin stained sections were prepared according to standard protocols to exclude background pathology interfering with experimental results. $ß_6$-integrin immunohistochemistry was performed as follows: After enzymatic antigen retrieval (Pronase E, 1:20 in tris-buffered saline), unspecific protein and peroxidase binding was blocked with 3% hydrogen peroxide and 3% normal goat serum (Abcam).

Immunohistochemistry was performed with a Dako autostainer using an antibody against the ß$_6$ subunit (1:50, Calbiochem, 407317). For antibody detection, biotinylated goat-anti-mouse secondary antibody (medac diagnostics, 71-00-29) was used, visualized by a streptavidine-peroxidase system (medac diagnostics, 71-00-38) and diaminobenzidine (immunologic, BS04-500). Counterstaining was done using hematoxylin.

RESULTS

Figure 1 shows that in combination with the previously reported TRAP(azide)$_3$ (*45*), newly synthesized TRAP derivatives with asymmetrical azide substitution pattern and additional polyethyleneglycol (PEG) linkers represent a valuable toolkit for straightforward click-chemistry synthesis of mono-, di, and trimeric peptide-chelator conjugates. The complementary terminal alkyne was introduced into the cyclic nonapeptide cyclo(FRGDLAFp(*N*Me)K) by amide formation with 4-pentynoic acid on the lysine side chain, resulting in the building block AvB6.

These components were used for straightforward CuAAC synthesis of four conjugates (Fig. 1), differing in the type of linker and the number of peptide copies (1–3) per molecule. The Cu^{II} which is inevitably complexed by TRAP in the course of CuAAC was subsequently removed by transchelation with 1,4,7-triazacyclononane-1,4,7-triacetic acid (NOTA) at pH 2.2 as described previously (*45*). In addition, functionalization of c(FRGDLAFp(*N*Me)K) with an aminohexyl linker and NODAGA (*46*), a bifunctional 1,4,7-triazacyclononane-1,4,7-triacetic acid derivative, afforded the conjugate NODAGA-AvB6 (Fig. 2) which possesses a high degree of structural similarity to the

TRAP-based monomer Avebehexin. Thus, a total of 5 c(FRGDLAFp(*N*Me)K) conjugates was available for evaluation—2 monomers, 1 dimer and 2 trimers.

αvβ6 integrin activity data shown in Table 1 confirms that functionalization of the cyclo(FRGDLAFp(*N*Me)K peptide on the lysine side chain indeed does not affect the binding affinity, as IC_{50} values of both monomers are similar to that of the non-decorated peptide (260 pM) (*33*). As expected for multimeric systems, activity is increased by a factor of ≈ 2 for the dimer ^{68}Ga-TRAP(AvB6)$_2$ and by a factor of ≈ 11 for the trimer ^{68}Ga-TRAP(AvB6)$_3$, relative to ^{68}Ga-Avebehexin.

Exchange of the free carboxylates of TRAP by peptide substituents also had a marked influence on overall polarity. While ^{68}Ga-Avebehexin is very hydrophilic (log *D* = –3.71), the dimer and trimer show a more lipophilic character (log *D* of –2.14 and –1.72, respectively; see Tab. 1). The lipophilicity induced by the multiple peptides could only be insufficiently compensated by introduction of PEG10-linkers. ^{68}Ga-TRAP(PEG10-AvB6)$_3$ exhibited a slightly improved log *D* (–1.94), albeit at the expense of a decreased αvβ6 integrin activity (87 vs. 23 pM). A total of 30 PEG units per molecule indeed effected a lower background uptake (Fig. 3).

However, a comparison of PET images for mono-, di-, and trimeric conjugates in the same mouse, bearing a subcutaneous H2009 (human lung adenocarcinoma) αvβ6 integrin-expressing tumor (Fig. 4), shows that clearance of the PEG-trimer was still far from being optimal. ^{68}Ga-TRAP(PEG10-AvB6)$_3$ and the dimer ^{68}Ga-TRAP(AvB6)$_2$ show much higher accumulation in the abdominal region (particularly in the liver area) than the monomers ^{68}Ga-NODAGA-AvB6 and ^{68}Ga-Avebehexin. A similar pattern was observed for kidney uptakes and general background. Unfortunately, the higher affinities of the

multimers did not effect a proportional increase of H2009 tumor accumulation, finally resulting in inferior tumor/organ contrast and a poor delineation of the tumor lesion (see Fig. 4A and B). Notwithstanding this, overall polarity appears not to be the only crucial parameter, as in-vivo properties of the monomers appear closely related despite their different $\log D$ values. The PET image obtained for the very hydrophilic ^{68}Ga-Avebehexin ($\log D$ = –3.71, Fig. 4D) is comparable to that of ^{68}Ga-NODAGA-AvB6 (see Fig. 4C), although the $\log D$ value of the latter is much closer to that of ^{68}Ga-TRAP(AvB6)$_2$ (–2.41 and –2.14, respectively).

The virtually complete lack of hepatobiliary excretion and the low background uptake rendered ^{68}Ga-Avebehexin the most attractive compound for further investigation. Figure 5 confirms that the H2009 tumor is clearly delineated despite only a fraction of tumor cells is positive for β6 integrin according to immunohistochemistry (Fig. 6), demonstrating high sensitivity of the tracer. Beyond that, it can be noticed that particularly the tumor cells adjacent to desmoplastic stroma show high β6 integrin expression in a membraneous and cytoplasmic pattern (Fig. 6B), highlighting the aforementioned link between αvβ6 integrin expression and epithelial-mesenchymal interaction.

PET and immunohistochemistry are well correlated with ex-vivo biodistribution data (Fig. 7). Apart from excretion-related elevated activity levels in the kidneys and urinary bladder, the highest uptake is found in the H2009 tumor, while the comparably low absolute value (0.65 %ID/g) is explained by the relatively low β6 integrin expression. Specificity is proven by a marked decrease of this signal upon co-injection of excess unlabeled compound (blockade), which can be seen as well in PET (Fig. 5A).

Some other blockable uptakes can be explained by a low but not entirely insignificant αvβ6 integrin expression in the epithelial cells of some internal organs. For example, immunohistochemistry confirmed that β6 integrin is weakly expressed by bronchial as well as alveolar epithelial cells in the lung (Fig. 6C) and by parietal cells in the glandular part of the mouse stomach (Fig. 6D). On the other hand, the pancreatic tissue, for example, shows no β6 integrin expression in any cellular compartment (Fig. 6E), resulting comparably insignificant uptake for both control and blockade. The immunohistochemistry furthermore corresponds essentially to the human expression patterns (*7*) and suggest that similar imaging results might be obtained in humans.

DISCUSSION

In order to facilitate interpretation of the in-vivo behaviour of the investigated compounds, it needs to be emphasized that high receptor affinity is a necessary, but not sufficient, condition for excellent in-vivo performance. Pharmacokinetics are largely determined by a compound's polarity and charge. A pronounced hydrophilicity promotes a fast excretion from non-target tissues via the kidneys and the urinary tract, which is desired for imaging probes. Concerning receptor affinities, it has been shown in numerous studies that tethering multiple copies of receptor ligands, for example, αvβ3 integrin targeting peptides of the cyclo(RGDXK) type, to a given reporter (e.g., radionuclide or fluorophor) is a reliable method to obtain constructs with increased integrin activity as well as higher uptake in αvβ3 integrin expressing tumors (*36,47,48,49,50,51,52,53,54*). The same was observed for α5β1 integrin tracers based on

a α5β1-specific pseudopeptide (*55*,*56*,*57*), suggesting that integrin-targeted radiopharmaceuticals might generally benefit from multimerisation. Thus, it appears somewhat counter-intuitive that in the present case, the best imaging results were obtained with the monomeric conjugates despite their lower αvβ6 integrin activities. We thus assume that the poor performance of the trimers is most probably a result of their lower degree of hydrophilicity, however more detailed investigations will be necessary to substantiate this hypothesis.

The excellent clearance from non-target tissues is the main reason why we consider ^{68}Ga-Avebehexin a top choice for clinical translation. The current results are underscoring the utility of mono-conjugated triazacyclononane-triphosphinate chelators with additional polar *P*-substitutents for improvement of hydrophilicity and renal clearance of ^{68}Ga radiopharmaceuticals (*58*,*59*). Although tumor uptake of ^{68}Ga-Avebehexin was quite low due to low target expression, it was found to be higher than in all other organs, in particular, lung, liver, stomach, and intestines (disregarding the kidneys wherein activity is concentrated owing to excretion). The pronounced target specificity and a decent tumor-to-background (i.e., muscle) ratio (10.8 ± 1.3, see Supplemental Table 1) rise high expectations regarding a clinical application of ^{68}Ga-Avebehexin for mapping of elevated αvβ6 integrin levels in epithelial tumors by PET. Particularly in view of the previously reported high expression of αvβ6 integrin in pancreatic adenocarcinoma (*7*), the high tumor-to-pancreas ratio (9.9 ± 1.6) suggests suitability for imaging of this type of tumor. Notwithstanding this, we would like to point out that more detailed investigations of pharmacodynamics, such as biodistribution data

for more time points, will be necessary to fully define the scope and limitations for ^{68}Ga-Avebehexin, which will be reported in due course.

CONCLUSION

For elaboration of tracers from targeting peptides, the fast, click-chemistry driven synthesis of substantially different types of conjugates for biological screening was shown to be an efficient way to identify the structural key parameters for a successful in-vivo transfer. In this respect, we like to emphasise that contrary to a large body of previous work, multimerisation did not work for the αvβ6 integrin-selective peptide c(FRGDLAFp(*N*Me)K). Although the multimers showed improved αvβ6 integrin affinities as expected, they did not exhibit improved target (i.e., tumor) accumulation in PET scans but instead, possessed inferior pharmacokinetics compared to the respective monomers.

Due to its excellent renal clearance and the resulting low background signal, the monomeric TRAP-conjugate ^{68}Ga-Avebehexin enabled highly sensitive PET imaging even of moderate αvβ6 integrin expression levels in subcutaneous H2009 (lung adenocarcinoma) xenografts in mice. It thus allows future in-vivo studies on some fundamental questions of tumor biology that recently caused an increasing interest in mapping αvβ6 integrin, such as the exact role of αvβ6 integrin overexpression and integrin-mediated epithelial-mesenchymal transition during tumor invasion, metastasis, and development of resistance to chemotherapies. Furthermore, we anticipate that ^{68}Ga-Avebehexin will prove clinically useful for specific PET imaging of cancers with high

αvβ6 integrin expression, such as pancreatic, ovarian, lung and gastric carcinoma as well as invasive head-and-neck carcinomas.

ACKNOWLEDGMENTS

Financial support (J.N.: by Deutsche Forschungsgemeinschaft, grant #NO822/4-1 and SFB 824, project Z1; K.S. and W.W.: by SFB 824, project Z2; H.K.: by Center of Integrated Protein Science Munich, CIPSM; T.G.K.: by International Graduate School of Science and Engineering, IGSSE) is gratefully acknowledged. The authors thank Markus Schwaiger for granting access to imaging devices; Sibylle Reder and Markus Mittelhäuser for assistance with animal PET; Alexander Wurzer, Martina Wirtz and Monika Beschorner for laboratory assistance.

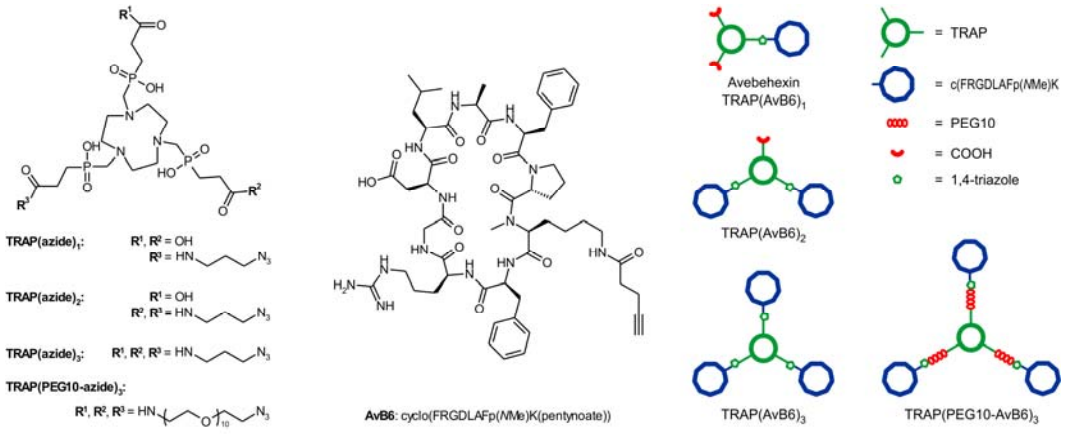

Figure 1: Building blocks used for synthesis of integrin αvβ6-targeted chelator conjugates by means of click chemistry (Cu-catalyzed azide-alkyne cycloaddition), and a schematic overview on integrin αvβ6 addressing chelator-peptide conjugates, obtained by CuAAC reaction. Reaction conditions: $Cu(OAc)_2 \cdot H_2O$ and sodium ascorbate in H_2O/MeOH, 1 h, room temperature. Workup (Cu removal) was done at pH 2.2, using 1,4,7-triazacyclononane-1,4,7-triacetic acid (NOTA) as scavenger. For exact structural formulae, see Supplemental Information.

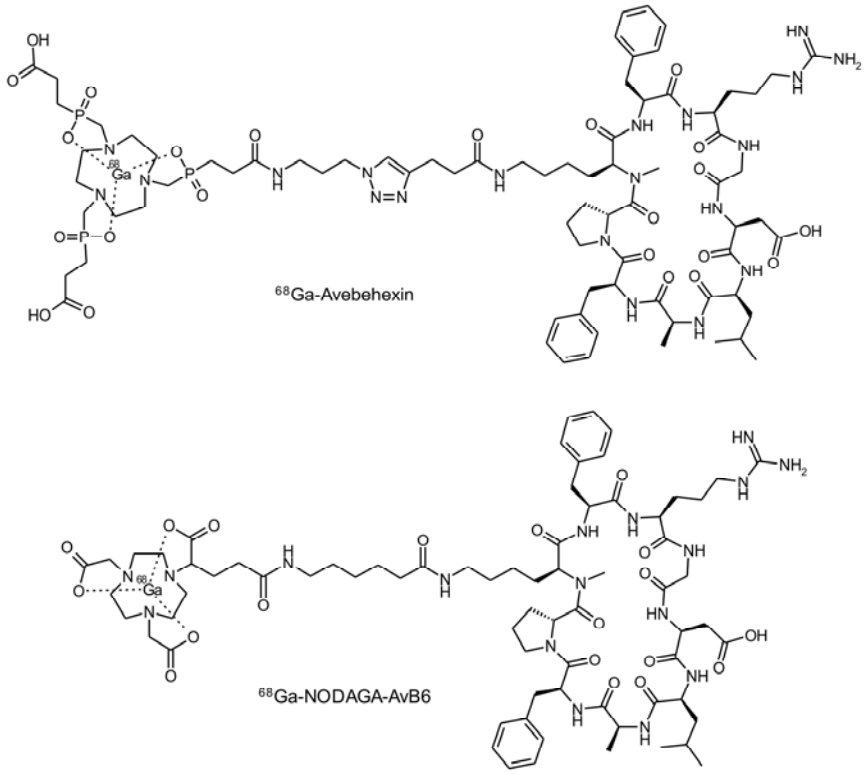

Figure 2: ^{68}Ga-Avebehexin and ^{68}Ga-NODAGA-AvB6, two gallium-68 labeled monomeric chelator conjugates of the peptide c(FRGDLAFp(NMe)K) for in-vivo mapping of integrin αvβ6 expression by PET.

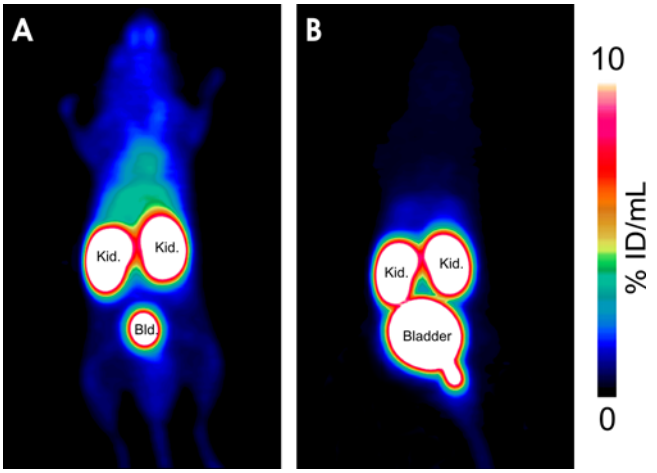

Figure 3: PET images (maximum intensity projections) of SCID mice recorded 75 min after administration of 20 MBq (1 nmol, 20 MBq/nmol) of ^{68}Ga-TRAP(AvB6)$_3$ (**A**) and ^{68}Ga-TRAP(PEG10-AvB6)$_3$ (**B**), illustrating the effect of PEG10 linkers in the side chains on overall pharmacokinetics.

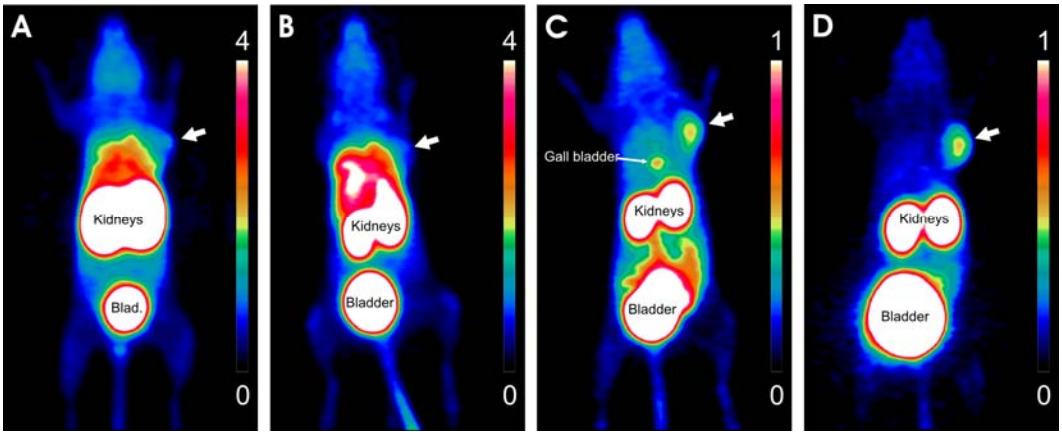

Figure 4: PET images (maximum intensity projections, 75 min p.i.) of a SCID mouse bearing a subcutaneous H2009 xenograft (human lung adenocarcinoma, position is indicated by white arrow), using approx. 15 MBq (0.3–0.4 nmol, 40–50 MBq/nmol) of ^{68}Ga-TRAP(PEG10-AvB6)$_3$ (**A**), ^{68}Ga-TRAP(AvB6)$_2$ (**B**), ^{68}Ga-NODAGA-AvB6 (**C**) and ^{68}Ga-Avebehexin (**D**). Scale bars indicate % injected dose per mL; note the different upper limits (4 for **A** and **B**, 1 for **C** and **D**).

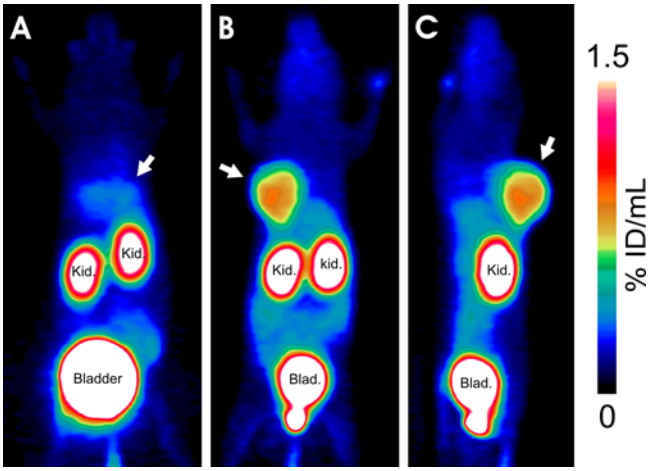

Figure 5: ^{68}Ga-Avebehexin-PET images (maximum intensity projections, 60 min p.i.) of two different H2009-bearing SCID mice, one with (blockade; **A**) and one without co-injection of 60 nmol Avebehexin (control; **B**, dorsal view and **C**, sagittal view; 12 MBq, 53 pmol, 230 MBq/nmol). H2009 tumor positions are indicated by white arrows.

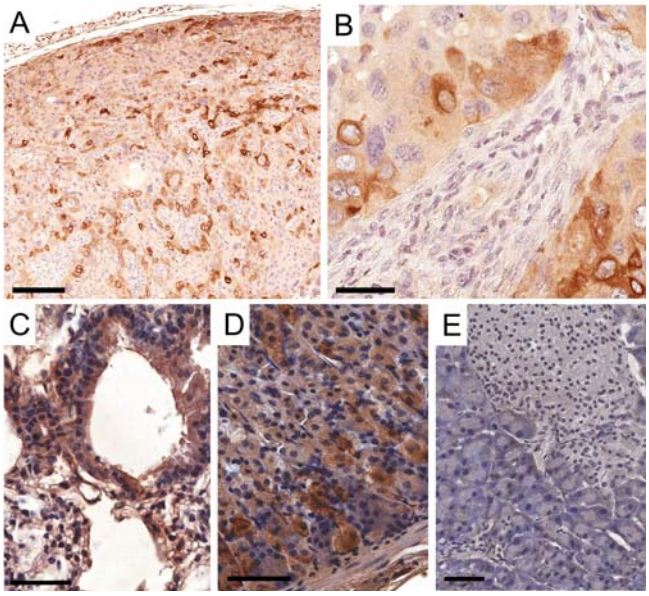

Figure 6: β6 integrin immunohistochemistry (IHC) of H2009 tumor (**A** and **B**), lung (**C**), glandular stomach (**D**), and pancreas (**E**) of the same animal used for control PET scans (Figure 5B and C). Bars indicate 200 µm (**A**) and 50 µm (**B**–**E**). Note that β6 integrin dimerises only with the αv chain, thus obviating a separate αv IHC for determination of actual αvβ6 distribution.

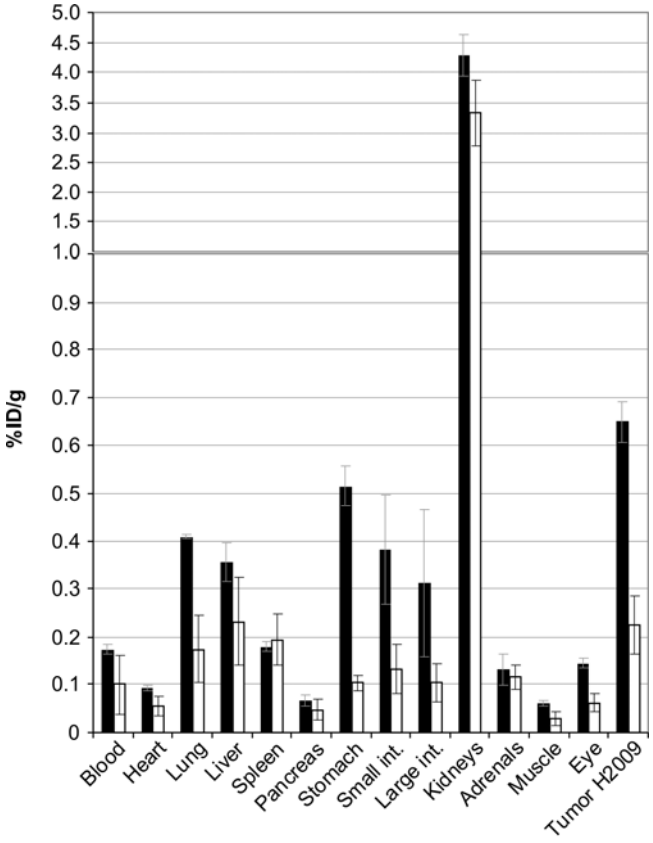

Figure 7: Biodistribution of approx. 12 MBq ^{68}Ga-Avebehexin in H2009 xenografted SCID mice, 90 min p.i., expressed as % injected dose per gram tissue; mean ± SD, n = 4. Black bars (control): 63 ± 10 pmol (190 ± 40 MBq/nmol); white bars (blockade): 64 ± 6 nmol (0.19 ± 0.02 MBq/nmol) (for data in numerical form and tumor/tissue ratios, see Supplemental Table 1).

Table 1: Octanol-PBS distribution coefficients (log *D*) and αvβ6 integrin affinities (expressed as 50% inhibition concentrations, IC_{50}) for ^{68}Ga-labeled αvβ6 integrin ligands. Affinities were determined using the non-radioactive $^{69/71}Ga^{III}$ complexes.

Compound	log *D*	IC_{50} [pM]
^{68}Ga-NODAGA-AvB6	–2.41 ± 0.05	267 ± 31
^{68}Ga-Avebehexin	–3.71 ± 0.03	260 ± 17
^{68}Ga-TRAP(AvB6)$_2$	–2.14 ± 0.11	120 ± 23
^{68}Ga-TRAP(AvB6)$_3$	–1.72 ± 0.04	23 ± 4
^{68}Ga-TRAP(PEG10-AvB6)$_3$	–1.94 ± 0.13	87 ± 12

REFERENCES

1 Margadant C, Monsuur HN, Norman JC, Sonnenberg A. Mechanisms of integrin activation and trafficking. *Curr Opin Cell Biol.* 2011:23;607–614.

2 Avraamides CJ, Garmy-Susini B, Varner JA. Integrins in angiogenesis and lymphangiogenesis. *Nat Rev Cancer.* 2008:8;604–617.

3 Breuss JM, Gillett N, Lu L, Sheppard D, Pytela R. Restricted distribution of integrin β6 mRNA in primate epithelial tissues. *J Histochem Cytochem.* 1993:41;1521–1527.

4 Niu G, Chen X. Why integrin as a primary target for imaging and therapy. *Theranostics.* 2011:1;30–45.

5 Krebs in Deutschland 2011/2012, 10. Ausgabe. Editors: Robert Koch-Institut and Gesellschaft der epidemiologischen Krebsregister in Deutschland e.V., Berlin, 2015.

6 Bandyopadhyay A, Raghavan S. Defining the role of integrin αvβ6 in cancer. *Curr Drug Targets.* 2009:10;645–652 .

7 Sipos B, Hahn D, Carceller A, et al. Immunohistochemical screening for β6-integrin subunit expression in adenocarcinomas using a novel monoclonal antibody reveals strong up-regulation in pancreatic ductal adenocarcinomas in vivo and in vitro. *Histopathol.* 2004;45:226–236.

8 Patsenker E, Wilkens L, Banz V, et al.The αvβ6 integrin is a highly specific immunohistochemical marker for cholangiocarcinoma *J Hepatol.* 2010;52:362–369.

9 Kawashima A, Tsugawa S, Boku A, et al. Expression of alphav integrin family in gastric carcinomas: increased αvβ6 is associated with lymph node metastasis. *Pathol Res Pract.* 2003;199:57–64.

10 Zhang ZY, Xu KS, Wang JS, et al. Integrin αvβ6 acts as a prognostic indicator in gastric carcinoma. *Clin Oncol.* 2008;20:61–66.

11 Arihiro K, Kaneko M, Fujii S, Inai K, Yokosaki Y. Significance of alpha 9 beta 1 and alpha v beta 6 integrin expression in breast carcinoma. *Breast Cancer.* 2000;7:19–26.

12 Ahmed N, Pansino F, Clyde R, et al. Overexpression of αvβ6 integrin in serous epithelial ovarian cancer regulates extracellular matrix degradation via the plasminogen activation cascade. *Carcinogenesis.* 2002;23:237–244.

13 Ahmed N, Riley C, Rice GE, Quinn MA, Baker S. αvβ6 integrin - a marker for the malignant potential of epithelial ovarian cancer. *J Histochem Cytochem.* 2002;50:1371–1380.

14 Bates RC, Bellovin DI, Brown C, et al. Transcriptional activation of integrin β6 during the epithelial-mesenchymal transition defines a novel prognostic indicator of aggressive colon carcinoma. *J Clin Invest.* 2005;115:339–347.

15 Ramos DM, But M, Regezi BL, et al. Expression of integrin β6 enhances invasive behavior in oral squamous cell carcinoma. *Matrix Biol*. 2002;21:297–307.

16 Wang B, Dolinski BM, Kikuchi N, et al. Role of αvβ6 integrin in acute biliary fibrosis. *Hepatology.* 2007;46:1404–1412.

17 Hahm K, Lukashev ME, Luo Y, et al. αvβ6 integrin regulates renal fibrosis and inflammation in Alport mouse. *Am J Pathol.* 2007;170:110–125.

18 Horan GS, Wood S, Ona V, et al. Partial inhibition of integrin αvβ6 prevents pulmonary fibrosis without exacerbating inflammation. *Am J Respir Crit Care Med.* 2008;177:56–65.

19 Goodman SL, Hölzemann G, Sulyok GA, Kessler H. Nanomolar small molecule inhibitors for αvβ6, αvβ5, and αvβ3 integrins. *J Med Chem.* 2002;45:1045–1051.

20 Kraft S, Diefenbach B, Mehta R, Jonczyk A, Luckenbach GA, Goodman SL. Definition of an unexpected ligand recognition motif for αvβ6 integrin. *J Biol Chem.* 1999;274:1979–1985.

21 Hausner SL, DiCara D. Marik J, Marshall JF, Sutcliffe JF. Use of a peptide derived from foot-and-mouth disease virus for the noninvasive imaging of human cancer: generation and evaluation of 4-[^{18}F]fluorobenzoyl A20FMDV2 for in vivo imaging of integrin αvβ6 expression with positron emission tomography. *Cancer Res.* 2007;67:7833–7840.

22 Li, S, Mcguire, MJ, Lin M, et al. Synthesis and characterization of a high-affinity αvβ6-specific ligand for in vitro and in vivo applications. *Mol Cancer Ther.* 2009;8:1239–1249.

23 Kimura RH, Teed R, Hackel BJ, et al. Pharmacokinetically stabilized cystine knot peptides that bind alpha-v-beta-6 integrin with single-digit nanomolar affinities for detection of pancreatic cancer. *Clin Cancer Res.* 2012;18:839−849.

24 Liu H, Wu Y, Wang F, Liu Z. Molecular imaging of integrin αvβ6 expression in living subjects. *Am J Nucl Med Mol Imaging.* 2014;4:333–345.

25 John AE, Luckett JC, Tatler AL, et al. Preclinical SPECT/CT imaging of αvβ6 integrins for molecular stratification of idiopathic pulmonary fibrosis. *J Nucl Med.* 2013;54:2146–2152.

26 Liu Z, Liu H, Ma T, et al. Integrin $\alpha v\beta_6$-Targeted SPECT Imaging for Pancreatic Cancer Detection. *J Nucl Med.* 2014;55:989–994.

27 Zhu X, Li J, Hong Y, et al. ^{99m}Tc-labeled cystine knot peptide targeting integrin αvβ6 for tumor SPECT imaging. *Mol Pharm.* 2014;11:1208–1217.

28 Hausner SH, Abbey CK, Bold RJ, et al. Targeted in vivo imaging of integrin αvβ6 with an improved radiotracer and its relevance in a pancreatic tumor model. *Cancer Res.* 2009;69:5843–5850.

29 Singh AN, McGuire MJ, Li S, et al. Dimerization of a phage-display selected peptide for imaging of αvβ6- integrin: two approaches to the multivalent effect. *Theranostics*, 2014;4:745–760.

30 Hausner SH, Bauer N, Sutcliffe JL. In vitro and in vivo evaluation of the effects of aluminum [^{18}F]fluoride radiolabeling on an integrin αvβ6-specific peptide. *Nucl Med Biol.* 2014;41:43–50.

31 Hausner SH, Bauer N, Hu LY, Knight LM, Sutcliffe JL. The effect of bi-terminal PEGylation of an integrin αvβ6-targeted ^{18}F-peptide on pharmacokinetics and tumor uptake. *J Nucl Med.* 2015;56:784–790.

32 Hausner SH, Carpenter RD, Bauer N, Sutcliffe JL. Evaluation of an integrin αvβ6-specific peptide labeled with [^{18}F]fluorine by copper-free, strain-promoted click chemistry. *Nucl Med Biol.* 2013;233:233–239.

33 Maltsev OV, Marelli UK, Kapp TG, et al. Stable peptides instead of stapled peptides: highly potent αvβ6-selective integrin ligands. A*ngew Chem Int Ed.* 2016;55:1535–1539.

34 Notni J, Šimeček J, Wester HJ. Phosphinic acid functionalized polyazacycloalkane chelators for radiodiagnostics and radiotherapeutics: unique characteristics and applications. *ChemMedChem.* 2014;9:1107–1115.

35 Notni J, Hermann P, Havlíčková J, et al. A triazacyclononane-based bifunctional phosphinate ligand for the preparation of multimeric 68Ga tracers for positron emission tomography. *Chem Eur J.* 2010;16:7174–7185.

36 Notni J, Šimeček J, Hermann P, Wester HJ. TRAP, a powerful and versatile framework for gallium-68 radiopharmaceuticals. *Chemistry*. 2011;17:14718–14722.

37 Šimeček J, Schulz M, Notni J, et al. Complexation of metal ions with TRAP (1,4,7-triazacyclononane-phosphinic acid) ligands and 1,4,7-triazacyclononane-1,4,7-triacetic acid: phosphinate-containing ligands as unique chelators for trivalent gallium. *Inorg Chem*. 2012;51:577–590.

38 Poty S, Désogère P, Šimeček J, et al. MA-NOTMP: A Triazacyclononane trimethylphosphinate based bifunctional chelator for gallium radiolabeling of biomolecules. *ChemMedChem*. 2015;10:1475–1479.

39 Šimeček J, Hermann P, Wester HJ, Notni J. How is ^{68}Ga-labeling of macrocyclic chelators influenced by metal ion contaminants in ^{68}Ge/^{68}Ga generator eluates? *ChemMedChem.* 2013;8:95–103.

40 Šimeček J, Zemek O, Hermann P, Wester HJ, Notni J. A monoreactive bifunctional triazacyclononane-phosphinate chelator with high selectivity for Gallium-68. *ChemMedChem.* 2012;7:1375–1378.

41 Máté G, Šimeček J, Pniok M, et al. The Influence of the combination of carboxylate and phosphinate pendant arms in 1,4,7-triazacyclononane-based chelators on their ^{68}Ga labeling properties. *Molecules*. 2015;20:13112–13126.

42 Notni J, Pohle K, Wester HJ. Comparative gallium-68 labeling of TRAP-, NOTA-, and DOTA-peptides: practical consequences for the future of gallium-68-PET. *EJNMMI Res*. 2012;2:28. (Communication)

43 Notni J, Hermann P, Dregely I, Wester HJ. Convenient synthesis of gallium-68 labeled gadolinium(III) complexes: towards bimodal responsive probes for functional imaging with PET/MRI. *Chemistry.* 2013;19:12602–12606.

44 Notni J, Plutnar J, Wester HJ. Bone seeking TRAP conjugates: surprising observations and implications on development of gallium-68-labeled bisphosphonates. *EJNMMI Res.* 2012;2:13. (Communication)

45 Baranyai Z, Reich D, Vágner A, et al. A shortcut to high-affinity Ga-68 and Cu-64 radiopharmaceuticals: one-pot click chemistry trimerisation on the TRAP platform. *Dalton Trans.* 2015;44:11137–11146.

46 Eisenwiener KP, Prata MIM, Buschmann I, et al. NODAGATOC, a new chelator-coupled somatostatin analogue labeled with [$^{67/68}$Ga] and [^{111}In] for SPECT, PET, and targeted therapeutic applications of somatostatin receptor (hsst2) expressing tumors. *Bioconjugate Chem.* 2002;13:530–541.

47 Šimeček J, Hermann P, Havlíčková J, et al. A cyclen-based tetraphosphinate chelator for preparation of radiolabeled tetrameric bioconjugates. *Chemistry.* 2013;19:7748–7757.

48 Thumshirn G, Hersel U, Goodman SL, Kessler H. Multimeric cyclic RGD peptides as potential tools for tumor targeting: solid-phase peptide synthesis and chemoselective oxime ligation. *Chemistry.* 2003;9:2717–2725.

49 Poethko T, Schottelius M, Thumshirn G, et al. Two-step methodology for high-yield routine radiohalogenation of peptides: ^{18}F-labeled RGD and octreotide analogs. *J Nucl Med.* 2004;45:892–902.

50 Dijkgraaf I, Kruijtzer JAW, Liu S, et al. Improved targeting of the αvβ3 integrin by multimerisation of RGD peptides. *Eur J Nucl Med Mol Imaging.* 2007;34:267–273.

51 Wängler C, Maschauer S, Prante O, et al. Multimerization of cRGD peptides by click chemistry: synthetic strategies, chemical limitations, and influence on biological properties. *ChemBioChem.* 2010;11:1–15.

52 Liu S. Radiolabeled Cyclic RGD peptides as Integrin αvβ3-targeted radiotracers: maximizing binding affinity via bivalency. *Bioconjugate Chem.* 2009;20:2199−2213.

53 Notni J, Pohle K, Wester HJ. Be spoilt for choice with radiolabeled RGD peptides: preclinical evaluation of ^{68}Ga-TRAP(RGD)$_3$. *Nucl Med Biol*. 2013;40:33–41.

54 Singh AN, Liu W, Hao G, et al. Multivalent bifunctional chelator scaffolds for gallium-68 based positron emission tomography imaging probe design: signal amplification via multivalency. *Bioconjugate Chem.* 2011;22:1650–1662.

55 D'Alessandria C, Pohle K, Rechenmacher S, et al. In vivo biokinetic and metabolic characterization of the 68Ga-labeled α5β1-selective peptidomimetic FR366. *Eur J Nucl Med Mol Imaging*. 2016;43:953–963.

56 Notni J, Steiger K, Hoffmann F, et al. Complementary, selective PET-Imaging of integrin subtypes α5β1 and αvβ3 using Ga-68-aquibeprin and Ga-68-avebetrin. *J Nucl Med.* 2016;57:460–466.

57 Notni J, Steiger K, Hoffmann F, et al. Variation of specific activities of Ga-68-aquibeprin and Ga-68-avebetrin enables selective PET-imaging of different expression levels of integrins α5β1 and αvβ3. *J Nucl Med.* 2016;57:1618–1624.

58 Šimeček J, Zemek O, Hermann P, Notni J, Wester HJ. Tailored gallium(III) chelator NOPO: synthesis, characterization, bioconjugation, and application in preclinical PET imaging. *Mol Pharmaceutics*. 2014;11:3893–3903.

59 Šimeček J, Notni J, Kapp TG, Kessler H, Wester HJ. Benefits of NOPO as chelator in gallium-68 Peptides, exemplified by preclinical characterization of ^{68}Ga-NOPO-c(RGDfK). *Mol Pharmaceutics*. 2014;11:1687–1695.

1. Biodistribution data for ^{68}Ga-Avebehexin

Supplemental Table 1: Biodistribution data (90 min p.i., n = 4) for ^{68}Ga-Avebehexin. Control: 63 ± 10 pmol; Blockade: 64 ± 6 nmol.

Organ/Tissue	^{68}Ga-Avebehexin		Blockade
	%ID/g	tumor/organ ratio	
blood	0.17 ± 0.01	3.7 ± 0.3	0.10 ± 0.06
heart (myocard)	0.09 ± 0.01	7.0 ± 0.4	0.06 ± 0.02
lung	0.41 ± 0.01	1.6 ± 0.1	0.17 ± 0.07
liver	0.36 ± 0.04	1.8 ± 0.1	0.23 ± 0.09
spleen	0.18 ± 0.01	3.6 ± 0.4	0.19 ± 0.05
pancreas	0.07 ± 0.01	9.9 ± 1.6	0.05 ± 0.02
stomach (empty)	0.52 ± 0.04	1.3 ± 0.1	0.10 ± 0.02
small intestine	0.38 ± 0.12	1.8 ± 0.6	0.13 ± 0.05
large intestine	0.31 ± 0.15	2.4 ± 0.9	0.10 ± 0.04
kidneys	4.29 ± 0.35	0.2 ± 0.0	3.33 ± 0.54
adrenals	0.13 ± 0.03	5.1 ± 1.1	0.12 ± 0.03
muscle	0.06 ± 0.00	10.8 ± 1.3	0.03 ± 0.01
eye	0.15 ± 0.01	4.5 ± 0.6	0.06 ± 0.02
tumor H2009	0.65 ± 0.04		0.22 ± 0.06

2. Chemical syntheses

Starting compounds and analytical methods

Unless otherwise noted, all reagents and solvents were of analytical grade. 3-azidopropylamine was purchased from Sigma-Aldrich. The H_2N-PEG(10)-azide linker was purchased from Iris Biotech (Marktredwitz, Germany; cat.# PEG3040). TRAP (1,4,7-triazacyclononane-1,4,7-tris[methylene(2-carboxyethyl)phosphinic acid], formerly named PrP9,[1] and TRAP(azide)$_3$[2] were synthesized as described previously. NOTA (1,4,7-triazacyclononane-1,4,7-triacetic acid) was purchased from CheMatech (Dijon, France). Analytical and preparative HPLC were performed on Shimadzu gradient systems with a SPD-20A dual wavelength UV/Vis detectors (220 nm, 254 nm). Eluents were

acetonitrile (J.T.Baker® Ultra Gradient HPLC grade, supplemented with 5% H_2O) and purified water (from Millipore system), each with 0.1% trifluoroacetic acid; gradient **A**: 15–65% MeCN in 20 min; gradient **B**: 5–55% MeCN in 20 min. Analytical HPLC was done on a Nucleosil 100-5 C18 column (125×4.6 mm), flow 1.0 mL min^{-1}. Preparative HPLC purification was done on a Multospher 100 RP 18-5µ column (250×10 mm), flow 5.0 mL min^{-1}. Mass spectra (ESI) were measured on a 500-MS Ion Trap spectrometer (Varian, by Agilent Technologies). pH values were measued with a SevenEasy pH-meter (Mettler Toledo, Gießen, Germany).

Generic synthesis protocol 1 (SP1)

For amide coupling on the terminal carboxylic acid groups of the TRAP chelator, TRAP (1.0 eq.) was dissolved in dry DMSO (ca. 0.5 M) and DIPEA (12 eq.). The respective amide (1.0 eq. for $n = 1$; 2.0 eq. for $n = 2$; 5.0 eq. for $n = 3$) was added quickly in one portion together with HATU ($n \times 3.0$ eq.) with stirring. After 60 min the reaction mixture was quenched with water, neutralized with trifluoroacetic acid (TFA) and directly subjected to preparative HPLC purification. Following removal of acetonitrile in vacuo, the aqueous eluate was lyophilized to yield the product as a TFA salt.

Generic synthesis protocol 2 (SP2)

For CuAAC conjugation to TRAP-azides, TRAP(azide)$_n$ (1.0 eq.) was dissolved in water (ca. 50 mM solution) and combined with a solution of the alkyne-functionalized peptide ($n \times 1.0$ eq.) in a small amount of MeOH. A solution of sodium ascorbate (0.5 M, 10–100 eq.) was added. Upon addition of an aqueous solution of $Cu(OAc)_2 \cdot H_2O$ (0.05 M, 1.2 eq.) a brown precipitate formed, which dissolved after stirring, resulting in a clear green solution. After 1 h, the reaction mixture was diluted to 3–4 mL (H_2O). For demetallation, 1,4,7-triazacyclononane-1,4,7-triacetic acid (NOTA, 12 eq.) was added, and 1 N aq. HCl was added in small portions until a pH of 2.2 was reached. After either 1 h at 60 °C, or 48 h at room temperature, the demetallation mixture was directly subjected to preparative HPLC purification. After removal of acetonitrile in vacuo, the aqueous eluate was lyophilized to yield the product as a TFA salt.

Synthesis of cyclo(FRGDLAFp(*N*Me)K(pentynoic acid) (AvB6)

Synthesis of the avb6-integrin targeting cyclic peptide was done as described previously.[3] Briefly, the linear peptide sequence *H*-**F**-**p**-(***N*Me)K**(Dde)-**F**-**R**(Pbf)-**G**-**D**(*t*Bu)-**L**-**A**-*OH* was synthesized according to standard Fmoc-Solid Phase Peptide Synthesis (SPPS) on a chloro-trityl polystyrene (CTC) resin. *N*-Methylation was performed on resin according to the previously reported method[4] with one exception: *N*-Nosyl protection was performed in dichloromethane (DCM) instead of *N*-methylpyrrolidine (NMP). The peptide is cleaved from the resin by incubation with a solution containing 20% HFIP/DCM for 10 min (3x). After backbone cyclization in DMF-solution using diphenyl phosphyl azide (DPPA) and $NaHCO_3$ as base, the Dde protecting group on the lysine side chain was cleaved off with hydrazine hydrate (2% solution in DMF). Precipitation by addition into in

brine yielded the peptide *c*(**FR**(Pbf)**GD**(*t*Bu)**LAFp**(*N*Me)**K**) (24.1 mg, 23 µmol) in good purity (>90% by HPLC, UV detection at 220 nm).

This material was reacted with pentynoic acid (2.7 mg, 27.6 µmol), HATU (10.5 mg, 27.6 µmol), HOAt (3.5 mg, 27.6 µmol) and DIPEA (11.7 µL, 69 µmol) in DMF. After 1 h at r.t., the solvent was removed in vacuo and the peptide was fully deprotected by addition of 2 mL of a mixture of 90% TFA, 5% DCM, 2.5% H_2O and 2.5% triisopropylsilane (TIPS). After After semipreparative HPLC purification (gradient: 25–34% acetonitrile in H_2O during 30 min) and lyophilisation, cyclo(FRGDLAFp(*N*Me)K(pentynoic acid) (**AvB6**) was obtained as a colourless solid (17.6 mg, 15.6 µM, 68 %).

Synthesis of NODAGA-AvB6

50 mg (1.0 eq., 37 µmol) of *c*(**FR**(Pbf)**GD**(*t*Bu)**LAFp**(*N*Me)**K**) (see previous paragraph) were reacted with Fmoc-Aminohexanoic acid (Fmoc-Ahx-OH) (1.2 eq., 15.5 mg, 44 µmol) with HATU (1.2 eq., 16.7 mg, 44 µmol), HOAt (1.2 eq., 5.6 mg, 44 µmol) and DIPEA (3.0 eq., 18 µL, 111 µmol) in DMF. After Fmoc deprotection of the linker with 20% piperidine in DMF, the peptide *c*(**Fp**(*N*Me)**K**(Ahx-*NH*$_2$)**FR**(Pbf)**GD**(*t*Bu)**LA**) was purified using semipreparative HPLC (gradient: 45–58% acetonitrile in H_2O during 26 min), 17.8 mg (33 µmol, 33%) yield.

14 mg (1.0 eq., 12.1 µmol) of this material was subsequently reacted with NODAGA(*t*Bu)$_3$ (1.5 eq. 7.9 mg, 14.5 µmol), HATU (5.4 mg, 1.2 eq.), and DIPEA (5 eq., 8.2 µL, 48 µmol) in DMF (1 mL). After removal of the solvent in vacuo, the conjugate was fully deprotected (reagent see above) within 5 h. HPLC purification (gradient: 28–39% acetonitrile in H_2O during 25 min) and lyophilisation afforded cyclo(FRGDLAFp(*N*Me)K(Ahx-NODAGA) (**NODAGA-AvB6**) as a colourless solid (10.6 mg, 7.0 µmol, 58%). MS (ESI, positive): *m*/*z* = 1516.5 [*M*+H$^+$], 759.1 [*M*+2H$^+$].

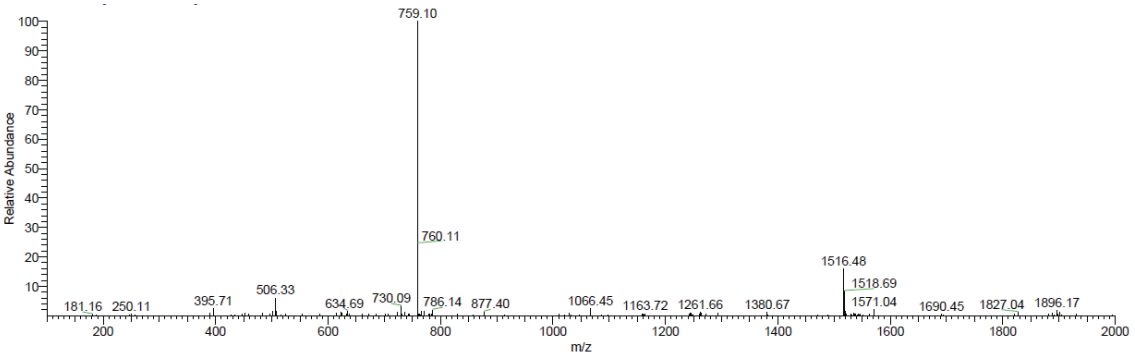

MS (ESI, positive) for NODAGA-AvB6

Synthesis of TRAP(azide)$_1$

TRAP (100 mg, 0.173 mmol, 1.0 eq.) and 3-azidopropylamine (17.3 mg, 17.0 µL, 0.173 mmol, 1.0 eq.) were reacted following procedure **SP1**, yielding TRAP(azide)$_1$·TFA (27.2 mg, 35.1 µmol, 20%) as a yellow hygroscopic solid. MW (calcd. for $C_{21}H_{42}N_7O_{11}P_3$): 661.53 HPLC (gradient: 3–40 %

MeCN in H_2O in 20 min): t_R = 6.5 min. ^{1}H-NMR (500 MHz, D_2O, 300 K): δ = 1.63 (p, 2H, $^3J_{HH}$ = 6.6 Hz, CH_2-C**H**$_2$-CH_2), 1.80–1.90 (m, 6H, (C(O)-C**H**$_2$), 2.30–2.36 (m, 2H, P^A-C**H**$_2$-C), 2.51 (dt, 4H, $^2J_{PH}$ = 13.0 Hz, $^3J_{HH}$ = 8.0 Hz, P^B-C**H**$_2$-C), 3.12 (t, 2H $^3J_{HH}$ = 7.0 Hz, N_3-C**H**$_2$), 3.21 (t, 2H, $^3J_{HH}$ = 5.5 Hz, N(H)-C**H**$_2$), 3.23 (d, 2H, $^2J_{PH}$ = 6.5 Hz, N-C**H**$_2$-P^A), 3.26 (d, 4H, $^2J_{PH}$ = 6.0 Hz, N-C**H**$_2$-P^B), 3.36–3.37 (m, broad, 12H, ring-C**H**$_2$) ppm*. ^{13}C{^{1}H}-NMR (125 MHz, D_2O, 300 K): δ = 25.11 (d, $^1J_{PP}$ = 95 Hz, P^B-**C**-C), 25.88 (d, $^1J_{PP}$ = 90 Hz, P^A-**C**-C), 26.70 (d, $^2J_{PP}$ = 3.8 Hz, P^B-C-**C**), 27.47 (C-**C**-C), 27.91 (d, $^2J_{PP}$ = 3.6 Hz, P^A-C-**C**), 36.70 (N(H)-**C**), 48.51 (**C**-N_3), 53.92 (d, $^1J_{PP}$ = 88 Hz, N-**C**-P^A), 54.58 (d, $^1J_{PP}$ = 89 Hz, N-**C**-P^B), 51.05 / 51.27 / 51.40 (three different ring-C), 174.67 (d, $^3J_{PC}$ = 13.7 Hz, N(H)-**C**=O^B), 177.38 (d, $^3J_{PC}$ = 13.0 Hz, **C**=O^A) ppm*. ^{31}P{^{1}H}-NMR (202 MHz, D_2O, 300 K): δ = 37.00 (P^B), 38.09 (P^A) ppm*. *: indices ^{A} and ^{B} indicate P and O atoms belonging to the undecorated^A and decorated^B side arm, respectively. MS (ESI, positive): *m*/*z* = 662.5 [*M*+H^+], 684.4 [*M*+Na^+].

Synthesis of TRAP(azide)$_2$

TRAP (1.0 eq.) was reacted with 3-azidopropylamine (2.0 eq.) following procedure **SP1**, yielding TRAP(azide)$_2$·TFA as a yellow hygroscopic solid. MW (calcd. for $C_{24}H_{48}N_{11}O_{10}P_3$): 743.64 HPLC (gradient **A**): t_R = 6.0 min. ^{1}H-NMR (500 MHz, D_2O, 300 K): δ = 1.61 (p, 4H, $^3J_{HH}$ = 6.7 Hz, CH_2-C**H**$_2$-CH_2), 1.83–1.92 (m, 6H, (C(O)-C**H**$_2$), 2.30–2.36 (m, 4H, P^A-C**H**$_2$-C), 2.51 (dt, 2H, $^2J_{PH}$ = 13.5 Hz, $^3J_{HH}$ = 7.5 Hz, P^B-C**H**$_2$-C), 3.11 (t, 4H, $^3J_{HH}$ = 7.0 Hz, N_3-C**H**$_2$), 3.21 (t, 4H, $^3J_{HH}$ = 6.5 Hz, N(H)-C**H**$_2$), 3.23 (d, 4H, $^2J_{PH}$ = 5.5 Hz, N-C**H**$_2$-P^A), 3.29–3.33 (m, broad, 14H, superposition of ring-C**H**$_2$ and d, N-C**H**$_2$-P^B) ppm*. ^{13}C{^{1}H}-NMR (125 MHz, D_2O, 300 K) δ = 24.76 (d, $^1J_{PP}$ = 95 Hz, P^B-**C**-C), 25.42 (d, $^1J_{PP}$ = 93 Hz, P^A-**C**-C), 26.62 (d, $^2J_{PP}$ = 3.9 Hz, P^B-C-**C**), 27.46 (C-**C**-C), 27.70 (d, $^2J_{PP}$ = 3.6 Hz, P^A-C-**C**), 36.71 (N(H)-**C**), 48.50 (**C**-N_3), 51.01 / 51.27 / 51.48 (three different ring-C), 53.89 (d, $^1J_{PP}$ = 88 Hz, N-**C**-P^A), 54.58 (d, $^1J_{PP}$ = 89 Hz, N-**C**-P^B), 174.46 (d, $^3J_{PC}$ = 14 Hz, N(H)-**C**=O^B), 177.39 (d, $^3J_{PC}$ = 12.3 Hz, **C**=O^A) ppm*. ^{31}P{^{1}H}-NMR (202 MHz, D_2O, 300 K) δ = 38.73 (P^B), 40.03 (P^A) ppm*. *: indices ^{A} and ^{B} indicate P and O atoms belonging to the undecorated^A and decorated^B side arm, respectively. MS (ESI, positive): *m*/*z* = 744.6 [*M*+H^+].

Synthesis of TRAP(PEG10-azide)$_3$

TRAP (50 mg, 86.3 µmol, 1.0 eq.) was reacted with H_2N-PEG10-N_3 (α-amino-ω-azido-decaethyleneglycol, 227 mg, 0.432 mmol, 5.0 eq.) following procedure **SP1**, yielding TRAP(PEG10-azide)$_3$·TFA (48.4 mg, 21.8 µmol, 25%) as a colourless hygroscopic oil. HPLC (gradient **A**): t_R = 8.5 min. MS (ESI, positive): *m*/*z* = 1053.8 [*M*+2H^+].

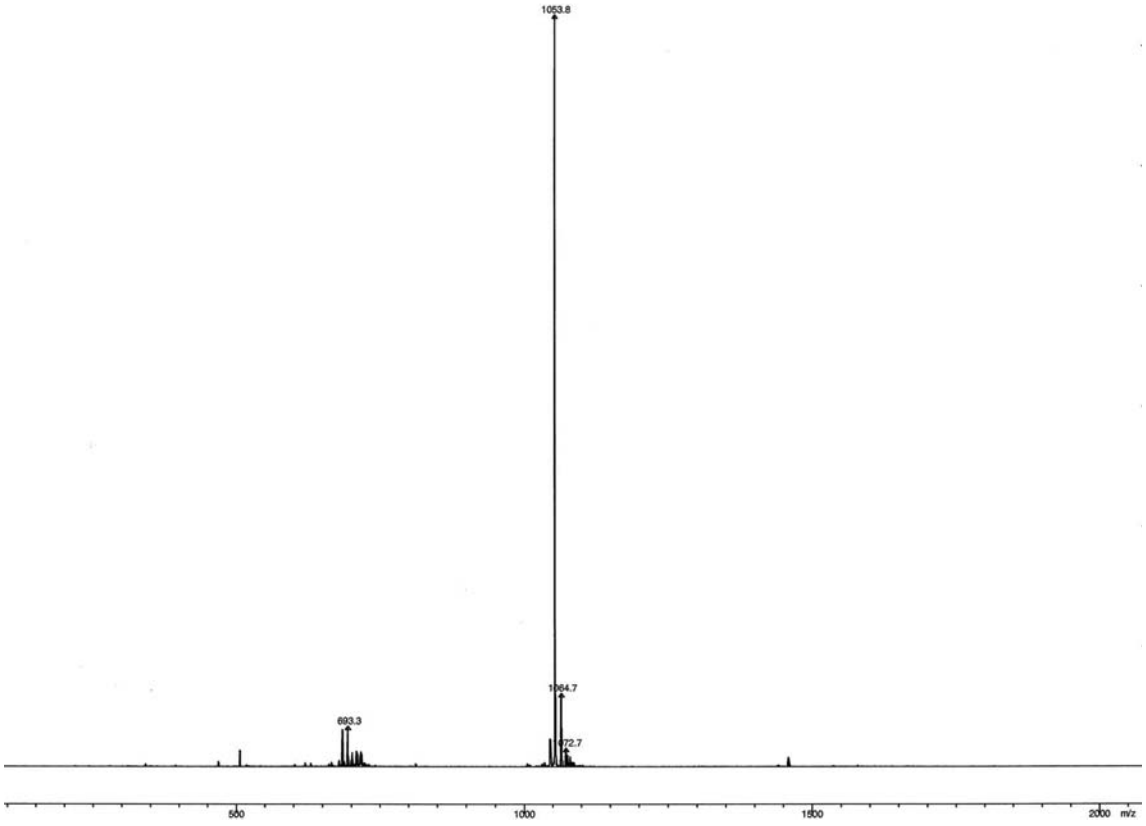

MS (ESI, positive) for TRAP(PEG10-azide)$_3$

Synthesis of Avebehexin

TRAP(azide)$_1$·TFA (3.4 mg, 4.4 µmol, 1.0 eq.) and AvB6 (5.0 mg, 4.4 µmol, 1.0 eq.) were coupled following procedure **SP2**, yielding the product TRAP(AvB6)$_1$·TFA (5.5 mg, 2.9 µmol, 66%) as a white solid. MS (ESI, positive): m/z = 1788.8 [M+H$^+$], 894.9 [M+2H$^+$], 597.1 [M+3H$^+$]. HPLC (gradient **B**): t_R = 11.5 min.

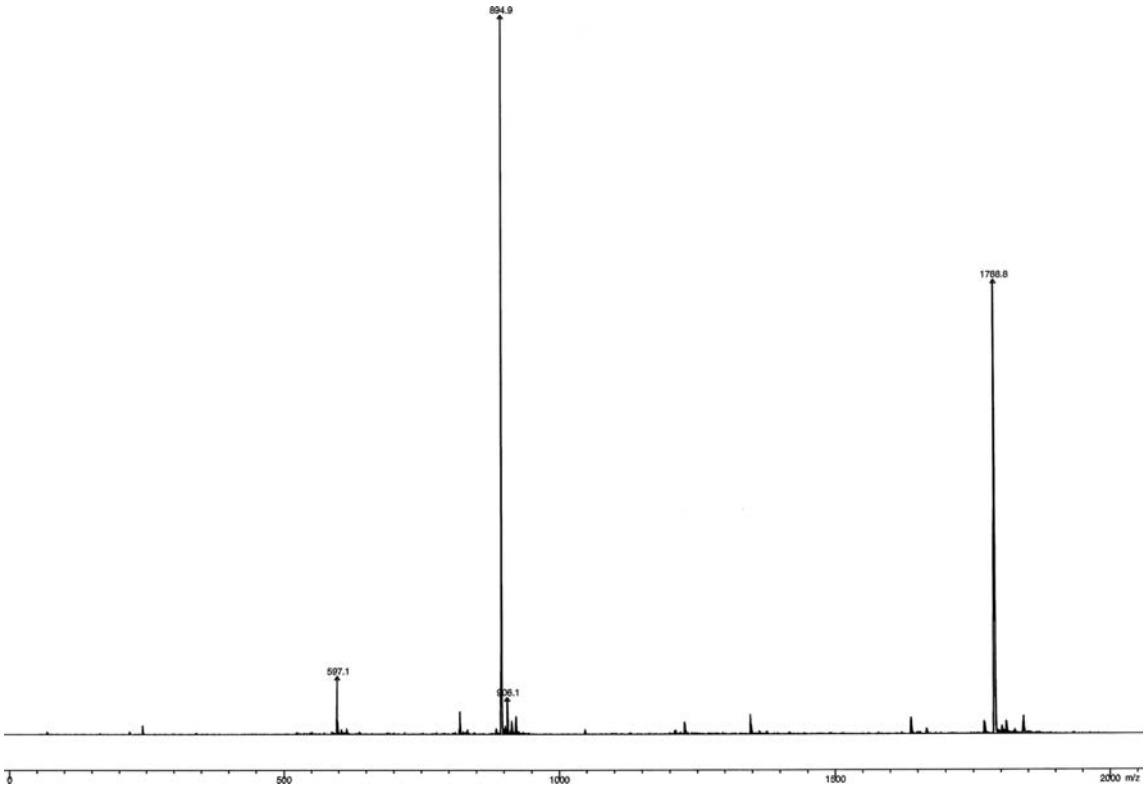

MS (ESI, positive) for Avebehexin

Synthesis of TRAP(AvB6)$_2$

TRAP(azide)$_2$·TFA (1.2 mg, 1.3 µmol, 1.0 eq.) and AvB6 (3.0 mg, 2.7 µmol, 2.0 eq.) were coupled following procedure **SP2**, yielding the product TRAP(AvB6)$_2$·TFA (1.0 mg, 0.31 µmol, 23%) as a white solid. MS (ESI, positive): m/z = 1499.4 [M+2H$^+$], 1000.5 [M+3H$^+$], 750.2 [M+4H$^+$]. HPLC (gradient **A**): t_R = 15.0 min.

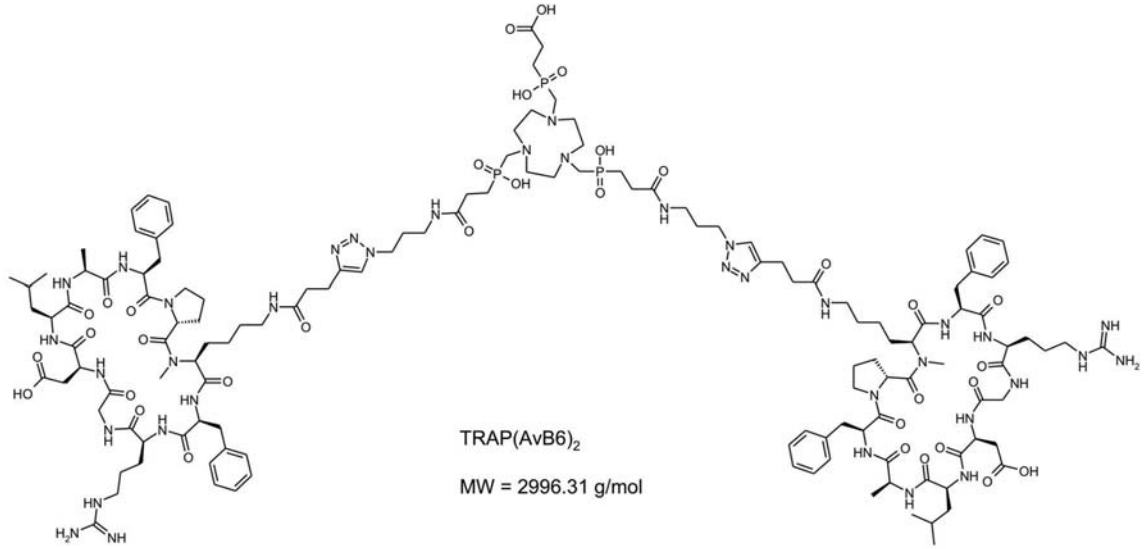

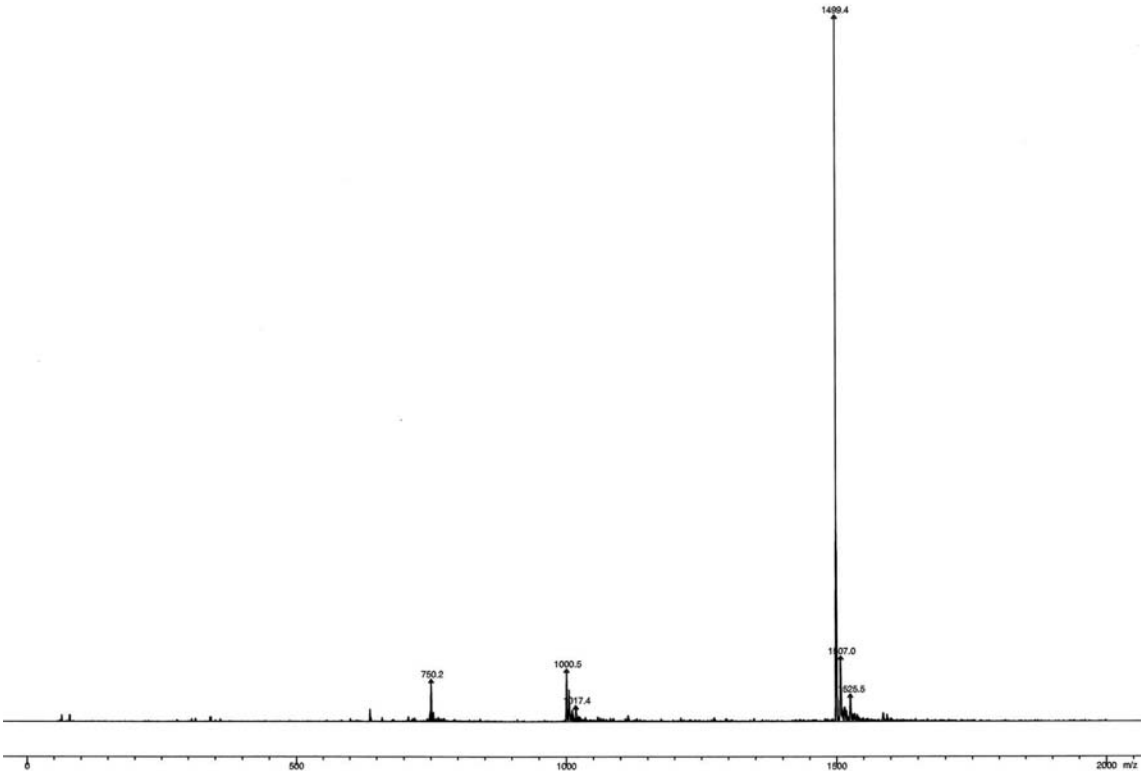

MS (ESI, positive) for TRAP(AvB6)$_2$

Synthesis of TRAP(AvB6)$_3$

TRAP(azide)$_3$·TFA (1.5 mg, 1.6 µmol, 1.0 eq.) and AvB6 (5.35 mg, 4.75 µmol, 3.0 eq.) were reacted following the procedure **SP2**, yielding the product TRAP(AvB6)$_3$·TFA (0.7 mg, 0.16 µmol, 10%) as a colorless solid. MS (ESI, positive): m/z = 1402.6 [M+3H$^+$], 1052.2 [M+4H$^+$]. HPLC (gradient **A**): t_R = 16.0 min.

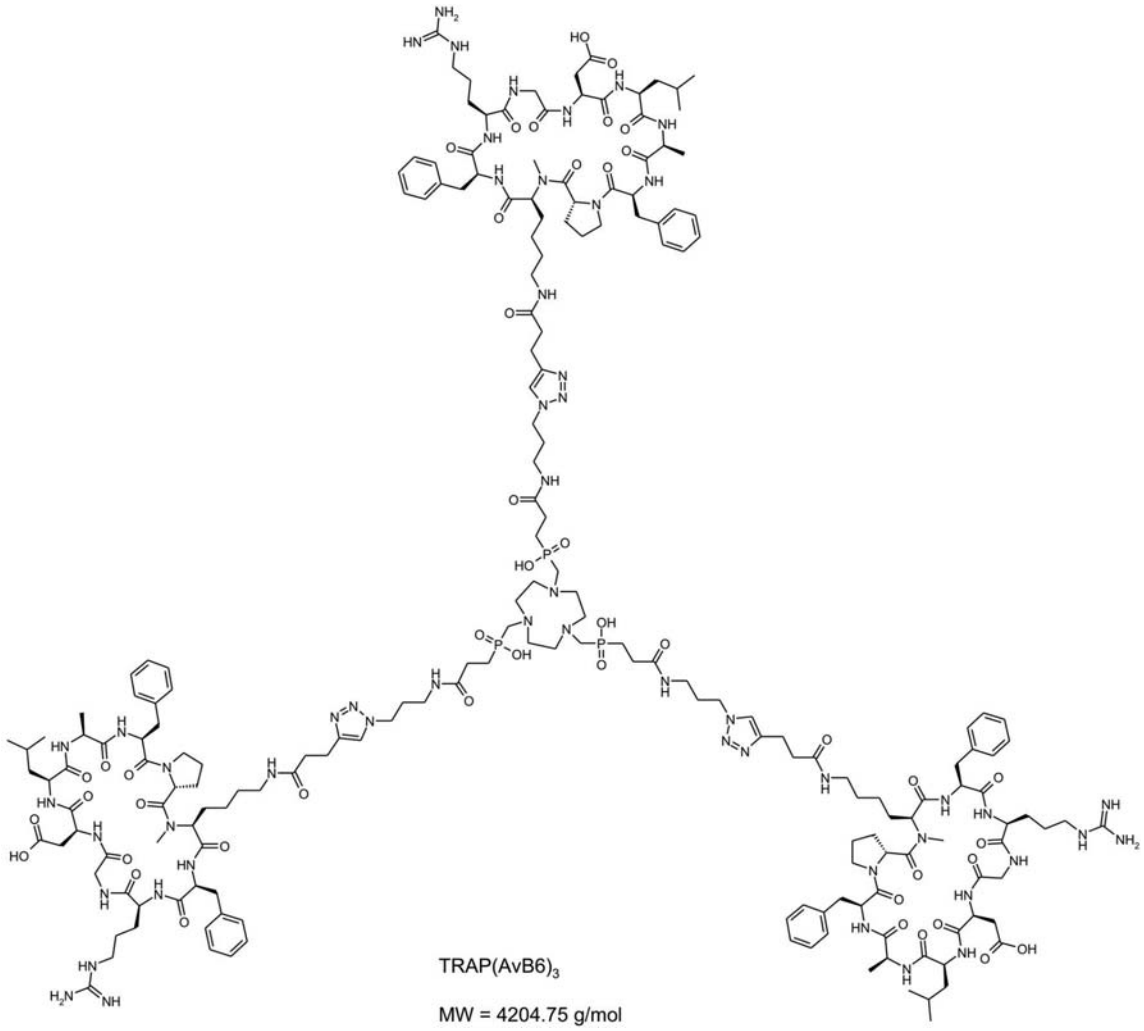

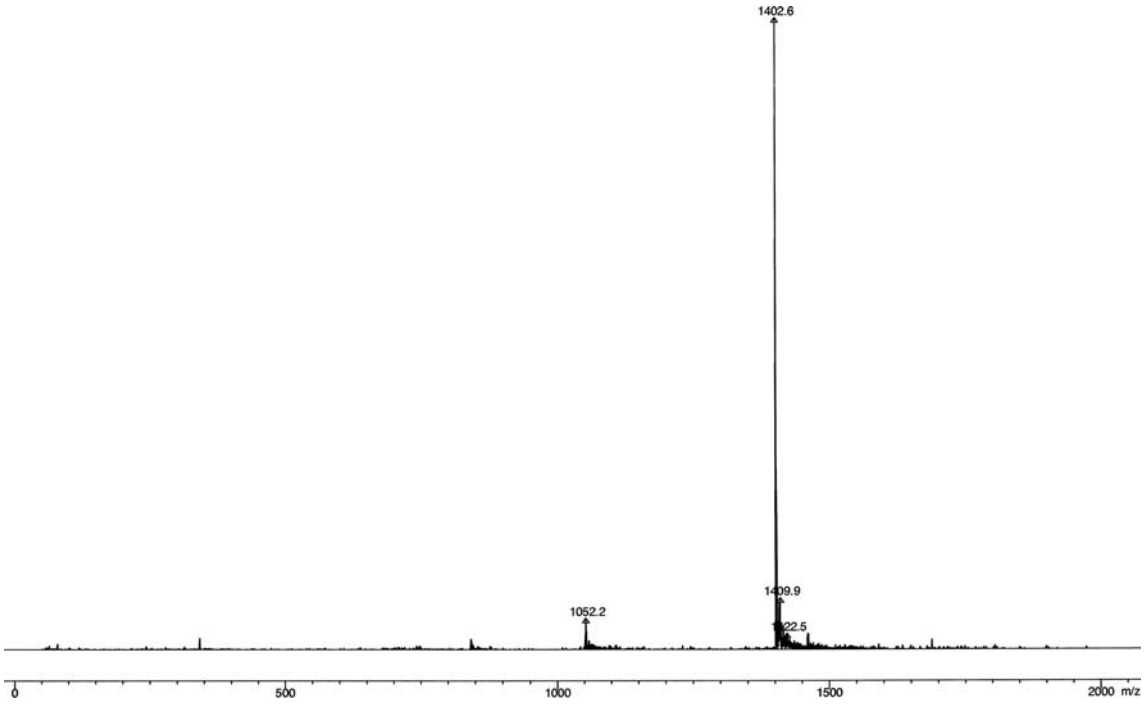

MS (ESI, positive) for TRAP(AvB6)$_3$

Synthesis of TRAP(PEG10-AvB6)$_3$

TRAP(PEG10-azide)$_3$·TFA (4.3 mg, 1.9 µmol, 1.0 eq.) and AvB6 (6.5 mg, 5.8 µmol, 3.0 eq.) were coupled following procedure **SP2**, yielding the product TRAP(PEG10-AvB6)$_3$·TFA (2.7 mg, 0.46 µmol, 24%) as a colorless oil. MS (ESI, positive): m/z = 1829.1 [M+3H$^+$], 1372 [M+4H$^+$], 1097.9 [M+5H$^+$], 915.1 [M+6H$^+$]. HPLC (gradient **A**): t_R = 16.5 min.

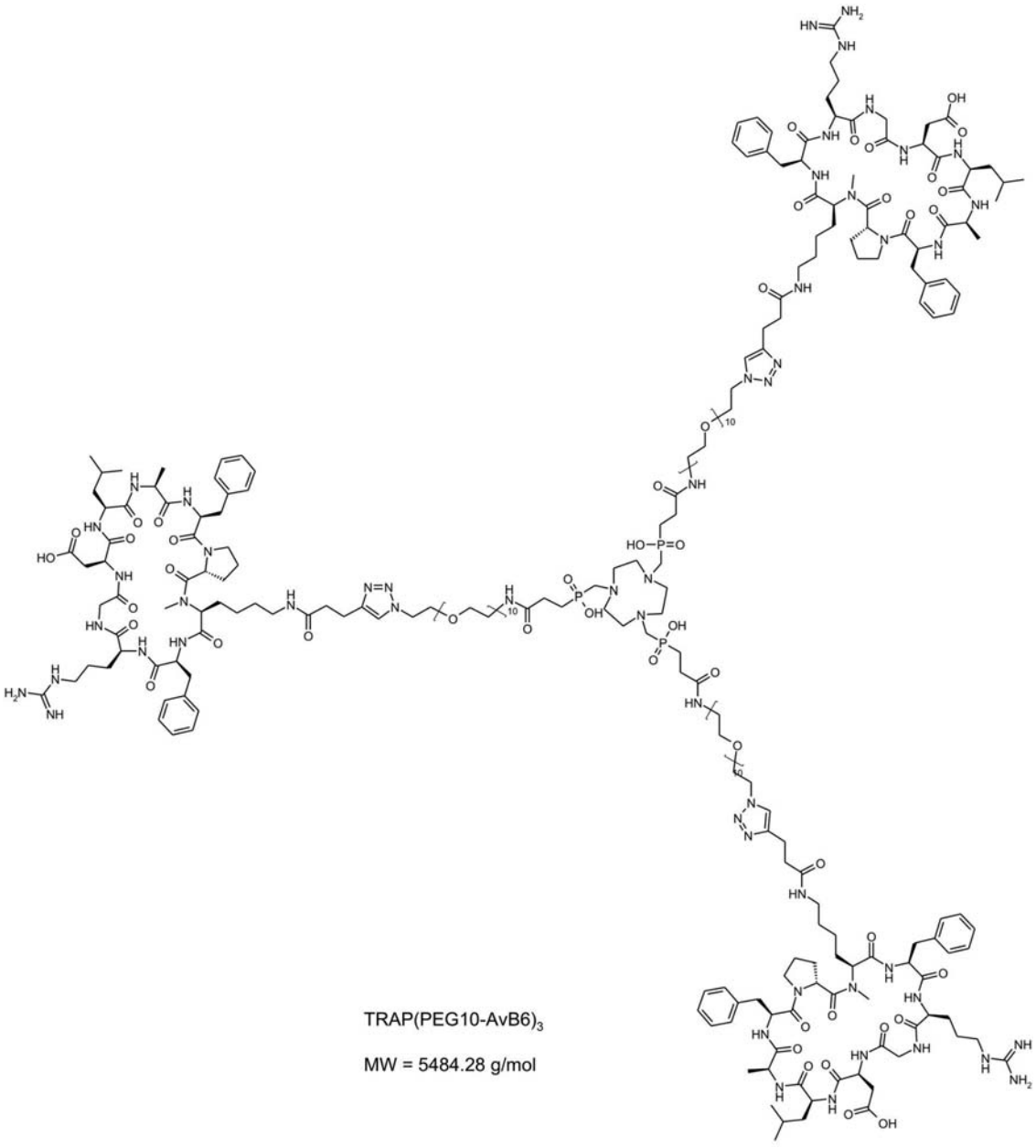

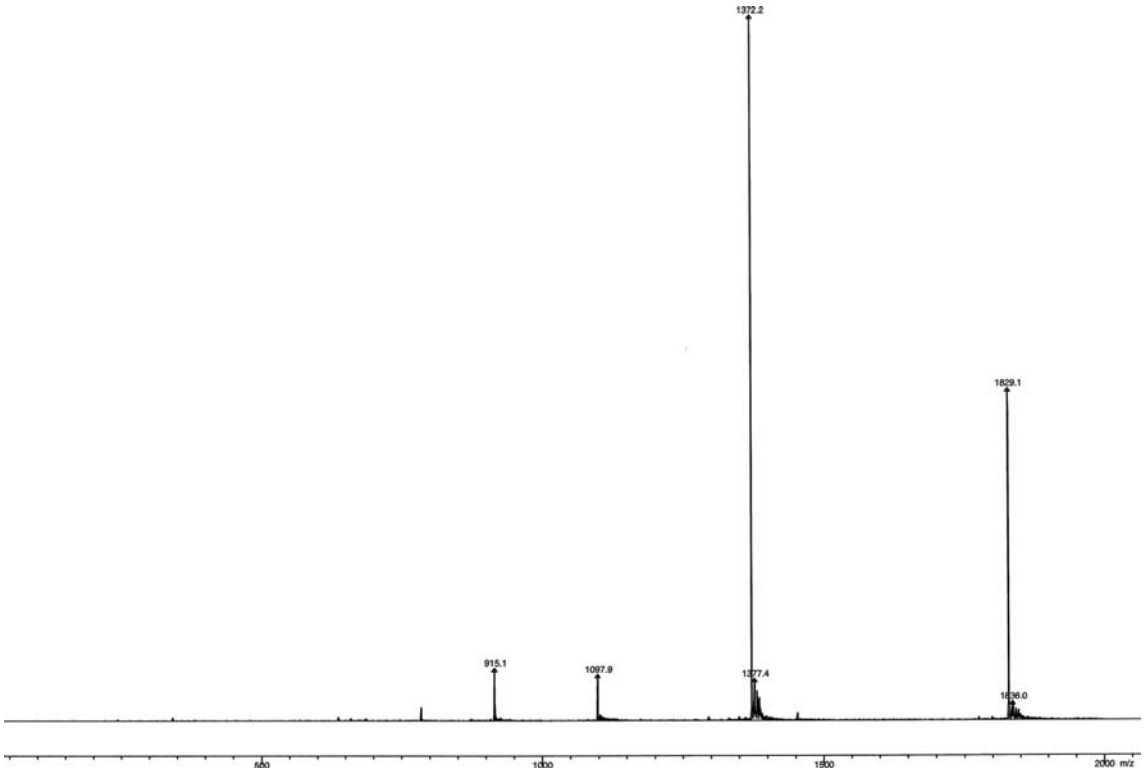

MS (ESI, positive) for TRAP(PEG10-AvB6)$_3$

References

1 J. Notni, P. Hermann, J. Havlíčková, J. Kotek, V. Kubíček, J. Plutnar, N. Loktionova, P. J. Riss, F. Rösch and I. Lukeš, *Chem. Eur. J.,* 2010, **16**, 7174–7185.

2 Z. Baranyai, D. Reich, A. Vágner, M. Weineisen, I. Tóth, H.-J. Wester and J. Notni, *Dalton Trans.,* 2015, **44**, 11137–11146.

3 O. V. Maltsev, U. K. Marelli, T. G. Kapp, F. S. Di Leva S. Di Maro, M. Nieberler, U. Reuning, M. Schwaiger, E. Novellino, L. Marinelli and H. Kessler, *Angew. Chem. Int. Ed.*, 2016, **55**, 1535–1539.

4 J. Chatterjee, B. Laufer, H. Kessler, *Nat.Protoc.* **201 2**, *7*, 432–444.